GLIDE OPTIMIZATION FOR CROSS COUNTRY WAVE FLIGHTS

By Scott A. Jenkins, Laurence Armi and Joseph Wasyl

Presented at the XXII OSTIV Congress, Uvalde, Texas, U.S.A. (1991)

ABSTRACT

We solve for optimal combinations of glide speeds and crab angles that minimize the glide slope at an arbitrary angle to the wind along a constant course heading. In this general case glide slope minimization is posed as a variational problem with both graphical and numerical solutions. The graphical solutions are obtained by tangent plotting of the along-course component of the glide polar for any constant crosswind component. The numerical solutions are obtained by seeded iterations with a Taylor series expansion about an analytic solution in the asymptotic limit of a small crosswind component. These solutions reveal that speeds-to-fly in severely oblique winds can actually increase with increasing tailwind component in order to avoid glide slope degradation from excessively large crab angles. Furthermore, indicated speeds-to-fly decrease with altitude in the absence of wind gradients aloft (as in absorption and insulation layers). On the other hand, if wind gradients are present aloft and obey Long's solution then indicated speeds-to-fly remain invariant with altitude. Within a lee wave field, it is shown that the glide slope between any two points is minimized by an orthogonal series of constant course glides proceeding crosswind through regions of lift and directly with or against the wind through regions of sink.

The solutions were also used to compute the flattest possible glide slopes that may be achieved across the spectrum of production sailplanes under a variety of extreme conditions. It was found that larger aspect ratios and low wing loadings have an increasing advantage with increasing tailwind and diminishing crosswind component. However, this advantage is greatly diminished with increasing headwind and crosswind components. Speed-to-fly and along course speeds segregated according to wing loading with tailwind and weak crosswind components, but varied inversely with wing thickness for oblique headwings and direct crosswinds. The practice of ballasting was shown to be advantageous for all oblique headwinds, direct crosswinds, and even in strong oblique tailwinds.

II NOMENCLATURE

A_0 = wing area, ft
A,B, = flight path way points
A',B',G = flight path way points
a,b,c = glide polar coefficients at altitude
$\hat{a}, \hat{b}, \hat{c}$ = glide polar coefficients at sea level
C_D = quadratic drag coefficient
$C_{D,i}$ = quadratic induced drag coefficient
$C_{D,p}$ = quadratic profile drag coefficient
C_L = quadratic lift coefficient
d_n, f_n = resolvent cubic parameters for iterative general solution
d_0, f_0 = resolvent cubic parameters for weak crosswinds
K_1 = profile drag factor
K_2 = induced drag factor
K_3 = glide polar factor due to profile drag
K_4 = glide polar factor due to induced drag
L/D = inverse glide slope
L/D_{max} = inverse glide slope due to speed-to-fly
L/D(u= U+δU) = inverse glide slope due to speed-to-fly errors
l = wing cord, nautical mi.
m = gross weight, lb
n = integral index number
p_n = second-order coefficient for general iterative case
p_0 = second-order coefficient for weak crosswinds
q_n = first-order coefficient for general iterative case
q_0 = first-order coefficient for weak crosswinds
R = Rossby radius of deformations, n.mi.
r_n = zero-order coefficient for general iterative case
r_0 = zero-order coefficient for weak crosswinds
S = air mass sink rate, kt
U = speed-to-fly altitude, kt
$\hat{U}$ = speed-to-fly at sea level in still air, kt
U_i = indicated speed-to-fly, kt
U_n = general speed-to-fly for nth wind increment, kt
U_0 = speed-to-fly in weak crosswinds, kt
u = horizontal component of glide velocity relative to air at altitude, kt
$\hat{u}$ = horizontal component of glide velocity relative to air at sea level, kt
u_s = stall speed, kt
v = wind speed, kt
v_0 = weak wind speed, kt
w = vertical component of glide velocity relative to air at altitude, relative sinking speed in knots
$\hat{w}$ = vertical component of glide velocity relative to air at sea level, relative sinking speed in knots
x = position along flight path relative to any given way point
α = wind angle relative to course line
β = crab angle relative to course line
γ = profile drag exponent
δU = speed-to-fly error, kt
δv = wind speed increment, kt
η = relative squared crosswind velocity difference, kt
θ = minimum glide slope in still air at sea level
λ = wave length, n. mi.
ρ = density at altitude, slug/ft^3
$\hat{\rho}$ = density at sea level, slug/ft^3

III INTRODUCTION

The first treatment of the problem of the glide speed that minimizes the glide slope in a moving atmosphere was due to MacCready (1954 and 1982). The solutions have since been referred to as "speed-to-fly." MacCready's original work was valid for a convective atmosphere in which regions of rising and sinking air translate horizontally with the wind. His speed-to-fly solutions were thus independent of the wind speed and determined uniquely by the rate of vertical air mass movement and the glide polar in still air at sea level.

Subsequently, Reichmann (1975 and 1978) and Kuettner (1985) considered the effects on glide slope minimization when regions of rising or sinking air do not translate with the wind over the ground. Such a condition is typically encountered in both hydrostatic and non-hydrostatic lee waves, see Gill (1982). Kuettner considered only the cases of glides directly with the wind. Reichmann presented a graphical orthogonalization for "Kurspolaren" when the wind is at an angle to the course heading. However, the tedious nature of this approach resulted in only a few example illustrations, with the complete family of speed-to-fly solutions and the optimal crab angles remaining unresolved. Even so, some striking departures from MacCready's original findings were uncovered by both authors in the case of a direct tailwind. Speed-to-fly was found to be dependent on the wind speed with the flattest glide slopes achieved for tailwinds at speeds less than the MacCready speed-to-fly. Kuettner also considered the degradation in glide slope at high altitudes. He concluded that the practice of ballasting to high wing loadings id disadvantageous since the reduced air density at high altitudes has already effectively raised the wing loading considerably. The increase in relative sinking speeds at these higher wing loadings cannot be compensated in downwind glides because slow speeds-to-fly are required.

In the present paper, the speed-to-fly problem is treated for the general case of glides along constant course headings at an arbitrary angle to the wind for any given altitude. Optimal flight paths for crossing lee waves are shown to result from an orthogonal series of constant course glides flown crosswind through regions of lift and along the wind through regions of sink. The orthogonal component glides flown along the wind are governed by the classical speed-to-fly theory, see Reichmann (1978). The crosswind orthogonal component glides are a particular case of the general solution for an arbitrary wind direction, as predominates outside the lee wave field. Here speed-to-fly is posed as a variational problem based on the assumption that the wind field varies slowly over geophysical length scales characteristic of lee waves and Rossby waves. In Section IV a graphical solution to the variational problem is developed around the concept of a "composite along-course polar" developed from the original Kurspolaren concept, but expanded to include computations of the optimal crab angle. The full family of speed-to-fly and optimal crab angle solutions, are then found in Section V by seeded iterations of the transcendental form of the speed-to-fly equation. The sensitivity of these solutions to variation in windspeed, direction, air mass sink and flight level is examined in Section VI. The results are also used in Section VII to explore the capabilities and speed-to-fly requirements for a wide range of production sailplanes in a number of critical wave soaring situations.

IV FORMULATION

Consider glides performed at 1-g load factor across a field of lee waves in such a manner that a constant course heading is maintained between any two arbitrary points (A,B), in an Eulerian frame. Let the course heading connecting (A,B) be at an angle α to the wind whose speed is v as shown in Figure 1. If the horizontal component of the glide velocity relative to the air is u, then it must be directed at some crab angle β in order to maintain a constant course heading between (A,B). The crab angle is thus given by:

$$\beta = \sin^{-1}[-(v/u)\sin\alpha] \qquad (1)$$

While traversing the lee wave field, regions of rising flow (lift) will be encountered along the upwind phases of the lee wave crests, and descending flow (sink) along the downwind phases. Let the vertical velocity component of the air mass be S, which shall be taken as positive in the downward direction in an Eulerian frame. If the vertical component of the glide velocity relative to the air is w (positive downward), then the inverse glide slope (L/D) with respect to an Eulerian frame such as the ground will be:

$$L/D = \frac{v\cos\alpha + u\cos\beta}{w + S} = \frac{v\cos\alpha + \sqrt{u^2 - v^2\sin^2\alpha}}{w + S} \qquad (2)$$

Here $v\sin\alpha$ is the crosswind component; $v\cos\alpha$ is the tailwind component; and $u\cos\beta$ is the along-course component of the glide velocity.

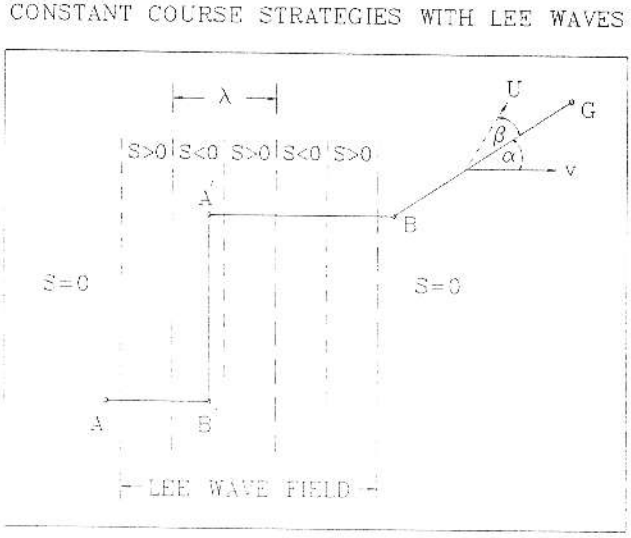

FIGURE 1. Schematic of cross country wave flights

Suppose a lee wave field lies between the two arbitrary points (A,B). The lee wave field structures the air mass sink rates in alternative parallel bands having high cross stream coherence as diagrammed schematically in Figure 1. Because of this feature, an orthogonal series of constant course glides yields the minimum glide slope between any two points (A,B), that are separated by some streamwise excursion. It is clear from inspection of equation 2 that straight line glides with a direct tailwind, $\alpha = 0$, give the maximum possible L/D (or flattest glide slope) when entering the lee waves along (A,B') or when traversing the lee wave field along (A',B). These two glides can be joined by a direct crosswind glide at constant course heading (B',A'), utilizing lee wave lift to achieve an infinite L/D when $S \rightarrow -w$. However, sufficiently long crosswind glides in uninterrupted lift such as (B',A') are not always possible. Variations in the alignment and width of wave generating mountains often destroy the necessary cross stream coherence of the lee wave field. If the ultimate goal is significantly far downwind, say G in Figure 1, then

skewed constant course glides such as (B,G) will become an inevitable part of cross country strategy.

The problem of optimizing glides skewed at an angle to the wind, such as (B,G) in Figure 1, appears to have been first been done graphically for a few selected cases by Huth (1963) with subsequent elaborations by Reichmann (1975). This method involves a vector projection of the glide polar along the course line, (B,G) for a given crosswind component, $v\sin\alpha$. This transforms the glide polar in still air, see Appendix 1, into a relation between a vertical component of the glide velocity, w, and the along-course component of the glide velocity, $u\cos\beta$, to yield the "Kurspolaren," or "along-course polar." Figure 2a gives examples of a number of these along-course polars for a practical range of crosswind components encountered in wave flights. The crosswind component remains constant over each of the along-course polars. The case of a zero crosswind component corresponds to the still air polar derived in Appendix 1. However, the crab angle, β varies continuously along each of the curves in Figure 2a. Along-course polars like Figure 2a can only resolve the crab angle after projecting from a given point along a line of constant sink rate, w, to the corresponding point on the still air polar in order to determine the glide speed, u; and then invoking equation 1 to calculate β.

To obtain a simultaneous graphical solution for both the speed-to-fly and the optimal crab angle in a glide skewed relative to the wind direction, we introduce a new type of along-course polar in Figure 2b. Here the sinking speed, w, is calculated as a function of the along-course speed, $u\cos\beta$, for constant crab angles. Therefore, the along-course polars in Figure 2b can only satisfy the constant course heading condition set forth in equation 1 if the crosswind component varies continuously along each curve. By themselves these are not particularly useful curves until combined with those in Figure 2a to yield the "composite along-course polars" plotted in Figures 3 and 4. Here, the along-course polars for constant crosswind components are plotted as solid lines while the along-course polars for constant crab angles are plotted as dashed lines. The along-course polars for a vanishing crosswind component and crab angle, $v\sin\alpha = \beta = 0$ are identically the still air glide polar derived in Appendix 1.

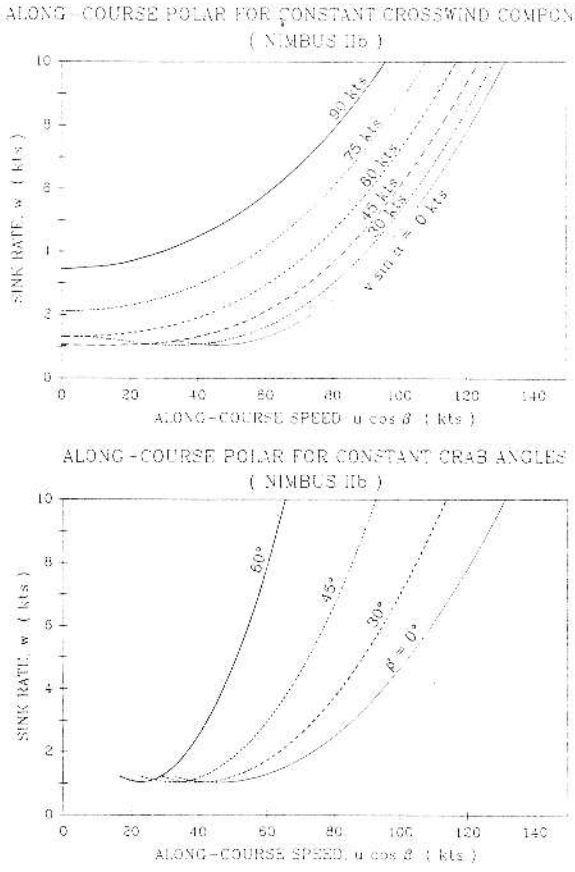

FIGURE 2: a) Along-course polars of a Nimbus IIb for constant crosswind components. The zero crosswind component (fine-solid) corresponds to the still air polar; b)Composite along-course polars of a Nimbus IIb for constant crab angles., The zero crab angle curve (fine-solid) corresponds to the still air polar.

To illustrate the methodology with this composite along-course polar consider the problem of a skewed glide in the absence of lift between points (B,G) in Figure 1 with a windspeed, $v = 72$ knots, and a wind angle, $\alpha = 56°$. The wind vector may therefore be decomposed into a tailwind component, $v\cos\alpha = 40$ knots, and a crosswind component, $v\sin\alpha = 60$ knots. According to equation 2, we offset the horizontal axis of the along-course polar by the tailwind component, $v\cos\alpha$ indicated by the solid circle in Figure 3. The flattest glide slope is given by a tangent line projected from the offset of the tailwind component to the corresponding along-course polar for a 60 knot crosswind component, as indicated by the dotted line in Figure 3. The tangent point indicated by the triangle is the along-course speed, $u\cos\beta$ giving the flattest possible glide slope for a 72 knot windspeed and 56° wind angle. For the actual speed-to-fly, we note the sink rate corresponding to this along-course speed and project along a line of constant sink rate to the still air polar. This constant sink rate projection is indicated by the dot-dash line in Figure 3, while the corresponding speed-to-fly of 68 knots is indicated by a square. To find the optimal crab angle, simply find which of the along-course polars for constant crab angle (dashed curves) passes through the tangent point of the along-course polar for constant crosswind component (solid line). In this case, that constant crab angle curve would be one just to the left of the 60° curve indicated in Figure 3, or 63°. For clarity, the along-course polar for a constant 63° crab angle has been omitted from Figure 3. If we consider the same problem in an air mass sinking at a rate of 1.5 knots, Figure 4, the tangent plotting procedure remains the same except that the point of projection is now displaced below the horizontal axis by 1.5 knots. The new solution gives a faster speed-to-fly, $U = 76$ knots, and a smaller optimal crab angle, $\beta = 52°$.

The graphical solutions for the speed-to-fly and the optimal crab angle using the composite along-course polars are useful for a few selected examples, and for understanding how the characteristics of the still air polar influence the particular nature of those solutions. However, this approach is highly inefficient and impractical for software applications in real-time air data computers or for generating look-up tables for a wide range of possible of windspeeds and directions. Moreover, the curves generated in Figures 3 and 4 are based on the still air polar at sea level. Consequently, it is necessary to generate additional sets of composite along-course polars for each altitude regime, based upon the altitude correction to the still air polar set forth in Appendix 1. The only way to circumvent this complication is to equip the sailplane with a non-altitude compensated variometer which reads low with increasing altitude by a factor equal to $\sqrt{p/\hat{p}}$, see Irving (1974). Then the indicated speeds-to-fly would be equivalent to those at sea level for any altitude. As an alternative to these difficulties, we present the following numerical variational solutions to the general speed-to-fly problem at an arbitrary angle to the wind.

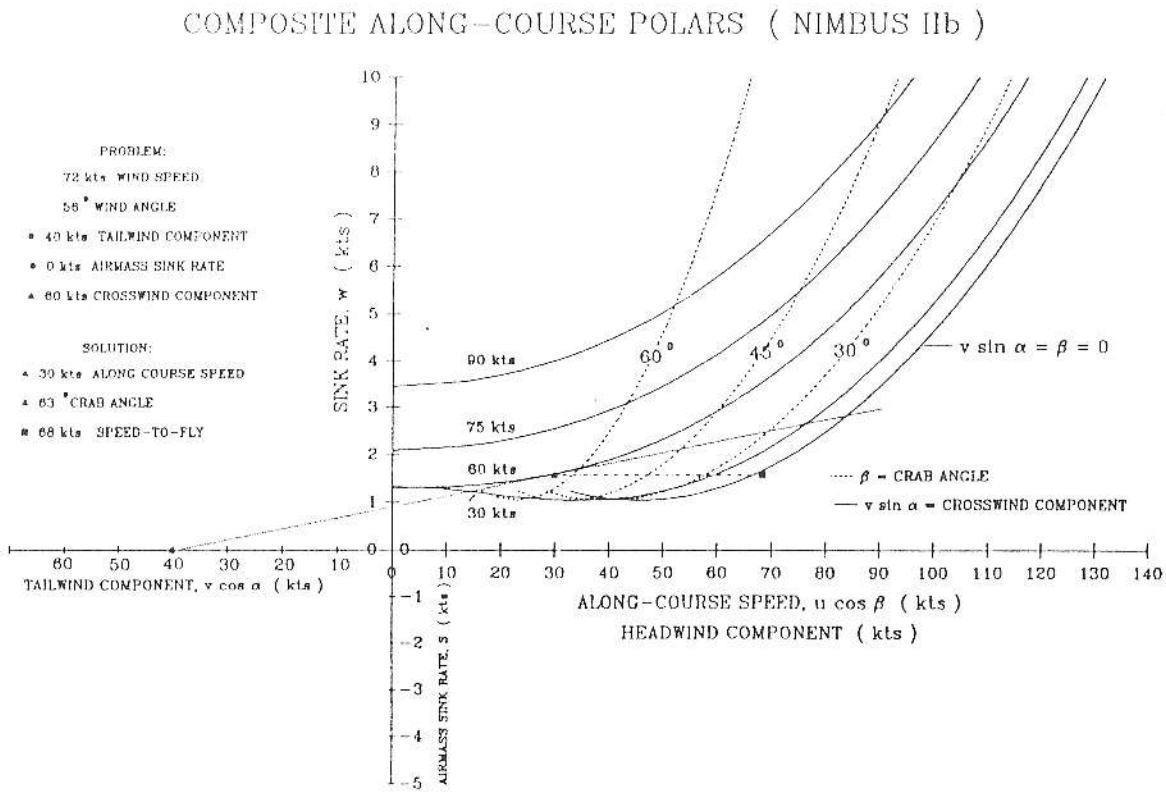

FIGURE 3: Composite along-course polars of a Nimbus IIb used to find the speed-to-fly and crab angle in a 72 knot oblique tailwind blowing at 56 degrees to the course line.

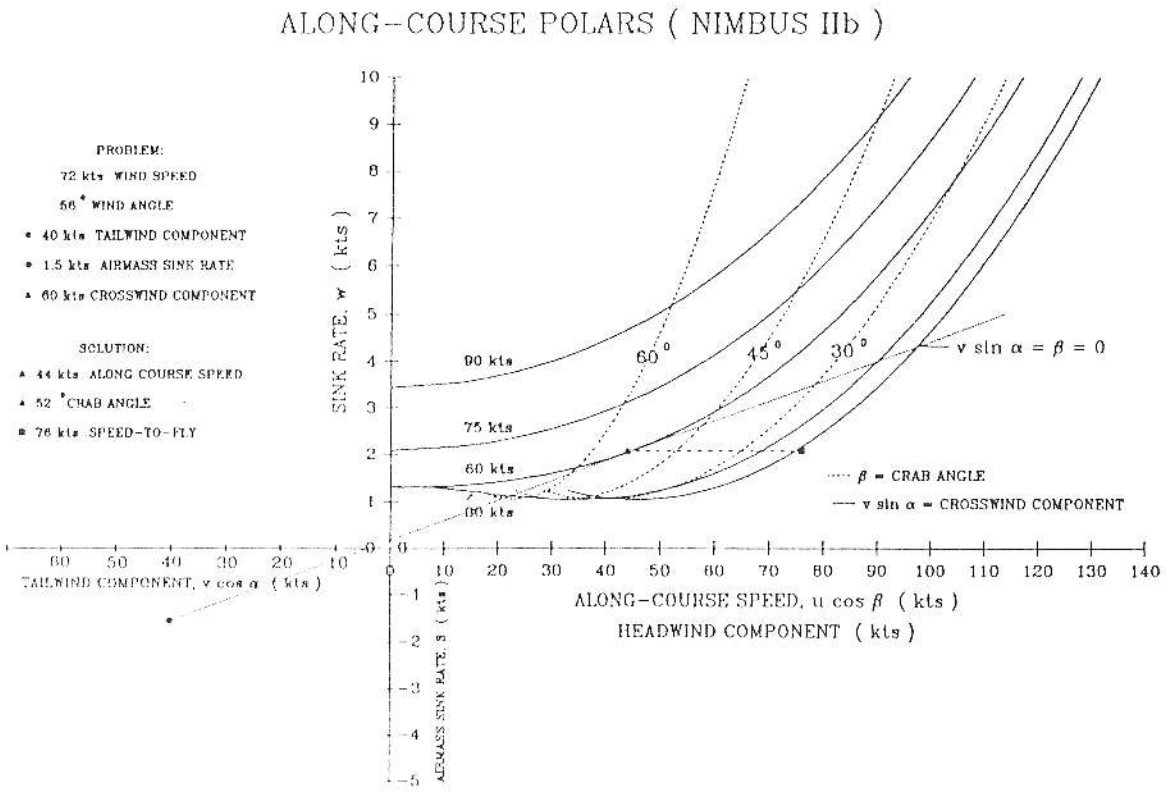

FIGURE 4: Composite along-course polars of a Nimbus IIb used to find the speed-to-fly and crab angle in a 72 knot oblique tailwind with 1.5 knots of sink.

V NUMERICAL VARIATIONAL SOLUTIONS

With equation 2 expressed in terms of equation 25 in Appendix 1, the inverse glide slope is reduced to dependence on four variables, u, v, α, S. Consequently, incremental changes in L/D are expressed as:

$$d(L/D) = \frac{\partial(L/D)}{\partial u}du + \frac{\partial(L/D)}{\partial v}dv + \frac{\partial(L/D)}{\partial \alpha}d\alpha + \frac{\partial(L/D)}{\partial S}dS \qquad (3)$$

Now, each of the variables in equation 3 changes with incremental changes in position along the flight path dx according to characteristic length scales. The air mass sink rates vary over distances comparable to the wave length, $O(\lambda/2\pi)$, of the lee waves. The wind speed and direction vary over the lowest mode length scales of the upper level storms, typically the Rossby radius of deformation, O(R), as discussed in Gill (1982). On the other hand, the horizontal component of the glide velocity can vary over distances of only a few cord lengths, O(nl), where n ~ 5 according to Basu and Hancock (1978). Therefore, the relative sizes of the terms in equation 3 are:

$$\frac{\partial(L/D)}{\partial u}du = \frac{\partial(L/D)}{\partial u}\frac{\partial u}{\partial x}dx = O\left(\frac{dx}{nl}\right) \qquad (4)$$

$$\frac{\partial(L/D)}{\partial v}dv = \frac{\partial(L/D)}{\partial v}\frac{\partial v}{\partial x}dx = O\left(\frac{dx}{R}\right) \qquad (5)$$

$$\frac{\partial(L/D)}{\partial \alpha}d\alpha = \frac{\partial(L/D)}{\partial \alpha}\frac{\partial \alpha}{\partial x}dx = O\left(\frac{dx}{R}\right) \qquad (6)$$

$$\frac{\partial(L/D)}{\partial S}dS = \frac{\partial(L/D)}{\partial S}\frac{\partial S}{\partial x}dx = O\left(\frac{2\pi\, dx}{\lambda}\right) \qquad (7)$$

In the atmosphere, R ~ O(100 n.mi.), whereas λ ~O(10 n.mi.) for hydrostatic lee waves or λ ~O(1 n.mi.) for non-hydrostatic lee waves. These are immense compared to the wing cord, l. Therefore, changes in L/D with respect to wind speed, direction, and air mass sink rate are negligible compared to those with respect to changes in glide speed over any incremental distance dx. Hence, the speed-to-fly, U, which maximizes the L/D over the ground, is given to $O(2\pi nl/\lambda)$ accuracy by

$$\frac{\partial}{\partial u}\frac{L}{D} = 0 \text{ at } u = 0 \qquad (8)$$

Equation 8 yields the general speed-to-fly equation for glides skewed relative to the wind, which may be written as

$$-aU^3 - 2avU\cos\alpha\sqrt{U^2 - v^2\sin^2\alpha} + (c + S + 2av^2\sin^2\alpha)U$$
$$- vb\cos\alpha\sqrt{U^2 - v^2\sin^2\alpha} + v^2b\sin^2\alpha = 0 \qquad (9)$$

The transcendental nature of the general speed-to-fly equation (equation 9) follows from the fact that speed-to-fly is a function of the crab angle by way of equations 2 and 8, and crab angle is, in turn, a function of speed-to-fly as required by equation 1. Analytic solutions to equation 9 arise in the asymptotic limit of an indefinitely small crosswind component, $U^2 > v^2\sin^2\alpha$, for which the speed-to-fly $u = U_o$ is given by:

$$U_o^3 + p_o U_o^2 + q_o U_o + r_o = 0 \qquad (10)$$

where

$$p_o = 2v_o\cos\alpha$$

$$q_o = [-(c + S + 2av_o^2\sin^2\alpha - v_o b\cos\alpha)/a]$$

$$r_o = (v_o^2 b\sin^2\alpha/a)$$

$$v_o = v < \sqrt{u_o^2/\sin^2\alpha}$$

The speed-to-fly equation thus collapses to an ordinary cubic equation for weak crosswinds, yielding the following solution:

$$U_o = \left[-\frac{d_o}{2} + \sqrt{\frac{d_o^2}{4} + \frac{f_o^3}{27}}\right]^{1/3} + \left[-\frac{d_o}{2} - \sqrt{\frac{d_o^2}{4} + \frac{f_o^3}{27}}\right]^{1/3} - \frac{2v_o\cos\alpha}{3} \qquad (11)$$

where

$$d_o = (1/27)(2p_o^3 - 9p_o q_o + 27r_o)$$

$$f_o = (1/3)(3q_o - p_o^2)$$

The remaining two roots of equation 10 are less than zero (backwards flight) and are, therefore, not sensible. As a particular case of equation 11, the speed-to-fly solution in a direct headwind or tailwind (α = 0), which corresponds to the graphical result by tangent plotting due to Kuettner (1985), is found to be

$$U_o(\alpha = 0) = (1/2a)[4a^2v^2 + 4a(c + S - bv)]^{1/2} - v \qquad (12)$$

For a general solution to equation 9 a seeded iteration is begun from the weak crosswind solution U_o for some small wind speed $v = v_o$. With each iterative step n thereafter, the wind speed is stepped incrementally by nδv. The numerical computations for any given step n are based on a Taylor series expansion of $(U^2 - v^2\sin^2\alpha)^{1/2}$ about the speed-to-fly solution from the previous iteration, $U = U_{n-1}$. By this numerical scheme, the general speed-to-fly equation for the nth iteration is

$$U_n^3 + p_n U_n^2 + q_n U_n + r_n = 0 \qquad (13)$$

where:

$$p_n = \frac{-vb\cos\alpha\left[\left(\frac{1}{2}\right)\eta^{\frac{-1}{2}} - \left(\frac{1}{2}\right)U_{n-1}\eta^{-3/2}\right] - 2av\cos\alpha\left(U_{n-1}^2\eta^{-3/2}\right)}{-a - av\cos\alpha\left(\eta^{-1/2} - U_{n-1}^2\eta^{-3/2}\right)} \qquad (14)$$

$$q_n = \frac{c+S+2av^2\sin^2\alpha - vb\cos\alpha U_{n-1}^2\eta^{\frac{-3}{2}} - 2av\cos\alpha\left[\eta^{\frac{1}{2}} - \left(\frac{1}{2}\right)U_{n-1}^2\eta^{\frac{-3}{2}} - (1/2)U_{n-1}^4\eta^{\frac{-3}{2}}\right]}{-a - av\cos\alpha\left(\eta^{-1/2} - U_{n-1}^2\eta^{-3/2}\right)} \qquad (15)$$

$$r_n = \frac{v^2 b\sin^2\alpha - vbc\cos\alpha\left[\eta^{1/2} - (1/2)U_{n-1}^2\eta^{-1/2} - (1/2)U_{n-1}^4\eta^{-3/2}\right]}{-a - av\cos\alpha\left(\eta^{-1/2} - U_{n-1}^2\eta^{-3/2}\right)} \qquad (16)$$

where $n = 1,2,3...$, $\eta = U_{n-1}^2 - v^2\sin^2\alpha$; and $v = v_o + n\delta v$. Hence, the general speed-to-fly solution for any given wind speed and arbitrary α is given by

$$U_n = \left[-\frac{d_n}{2} + \sqrt{\frac{d_o^2}{4} + \frac{f_n^3}{27}}\right]^{1/3} + \left[-\frac{d_n}{2} - \sqrt{\frac{d_o^2}{4} + \frac{f_n^3}{27}}\right]^{1/3} - \frac{2v\cos\alpha}{3} \qquad (17)$$

where $d_n = (1/27)(2p^3{}_n - 9p_n q_n + 27r_n)$; $f_n = (1/3)(3q_n - p^2{}_n)$; $n = 1,2,3....$ Again, the two remaining roots to equation 13 are less than zero and consequently have no physical significance.

VI NUMERICAL RESULTS

The general speed-to-fly solutions for arbitrary wind speed and direction were computed between the 700- and 300- mb levels by seeded iterations using equations 14-17. The computations were based on an unballasted Nimbus IIb glide polar according to Appendix 1. The computational sweeps were stepped in both the positive and negative wind directions using increments of $\delta v = 1.0$ knot. This procedure was selected in preference to some general iterative search routine because the speed-to-fly equation (equation 9) has multiple roots and it was desirable to find cause and effect relationships between speed-to-fly, optimal crab angle, air mass movements, and altitude effects on the glide polar. The speed-to-fly and optimal crab angle dependence on the wind speed and direction is computed in Figure 5 for the 700- mb level and in Figure 6 for the 300- mb level. These computations assume no net vertical motion in the atmosphere, S = 0, as would generally be the case during long glides between wave generating mountains. Negative wind speeds correspond to headwinds, whereas positive values denote tailwinds. Positive crab angles denote deviations from the

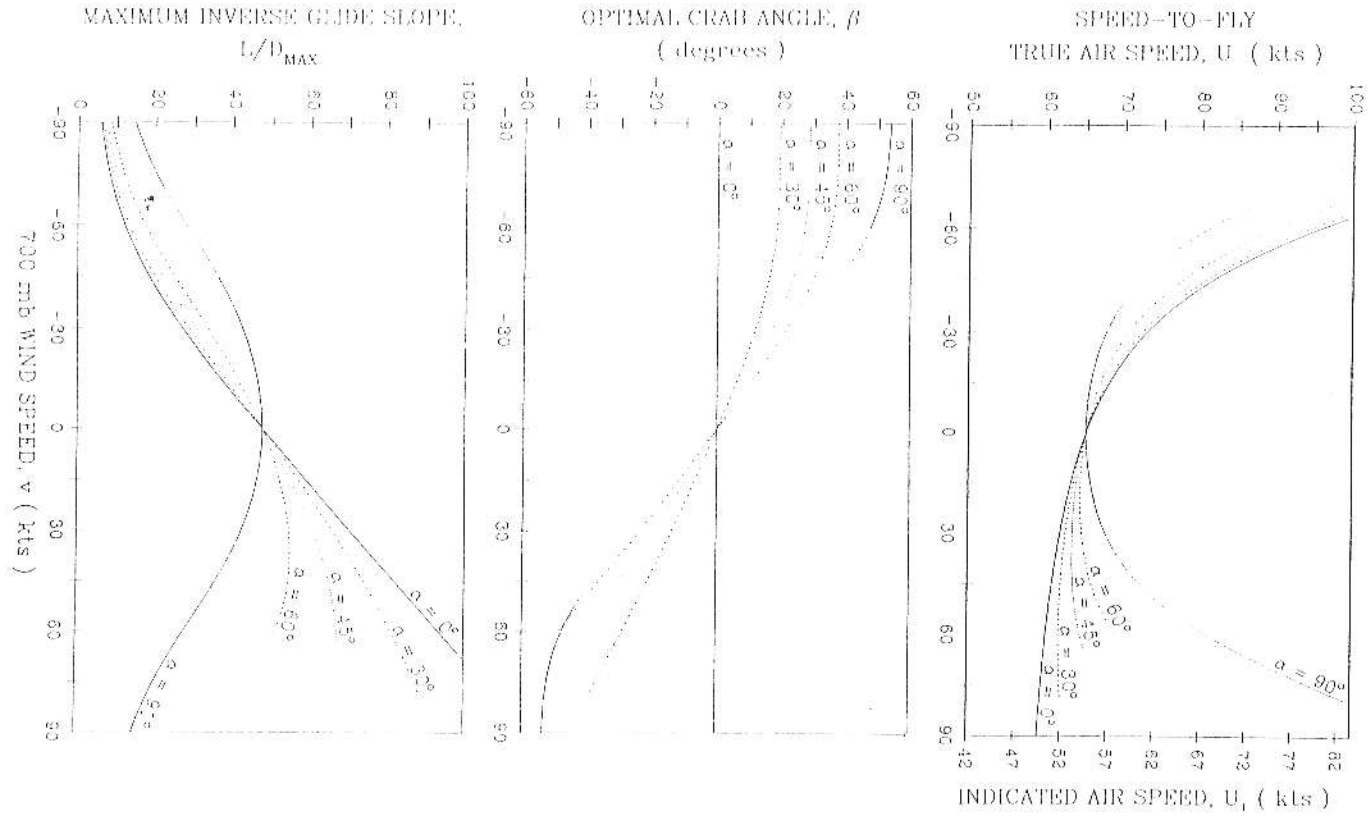

FIGURE 5: a) Speed-to-fly in the absence of lift as a function of wind speed and direction at the 700-mb level, (10,000 ft MSL); b) Optimal crab angle in the absence of lift as a function of wind speed and direction at the 700-mb level (10,000 ft MSL); c) Maximum obtainable L/D in the absence of lift as a function of wind speed and direction at the 700-mb level (10,000 MSL).

course line in the same sense as the wind angle (headwinds), whereas negative crab angles deviate from the course line against the wind angle (tailwinds). The fastest and slowest speeds-to-fly arise from glides directly against and with the wind ($\alpha = 0$), respectively. The speed-to-fly in a direct crosswind ($\alpha = 90°$) is a symmetric function about zero wind speed and is slower than all other headwind cases and faster than all other tailwind cases. All remaining possible crosswind solutions are intermediate between these two extremes, with small differences among oblique glides into the wind, but significantly faster speeds-to-fly for increasing crosswind components with the wind. Except for direct crosswinds or extremely oblique wind angles, $\alpha > 60°$ the maximum inverse glide slopes apparently result from keeping the crab angle small, less than O(45°). Hence, the speeds-to-fly during oblique glides with the wind increase with increasing crosswind component in order to maintain the course line without resorting to exceedingly large crab angles.

From comparisons of Figures 5a and 6a it is interesting to find that the indicated speed-to-fly (based on pitot-static airspeed systems) varies with altitude for any given wind speed and direction. This effect was not considered by MacCready (1954 and 1982). Generally, slower indicated airspeeds are required at higher altitudes for any constant non zero wind speed regardless of direction. In practice, the validity of this statement relies on the absence of a vertical wind gradient, as is typical of insulation layers aloft. Usually, wind gradients are present aloft, and many of these appear to obey Long's solution, see Gill (1982). If the lee-wave fields obey Long's solution, then the momentum flux of the wind remains constant, and the wind speed will increase with altitude as the square root of the density ratio, $(\hat{p}/p)^{1/2}$. Under conditions for Long's solution, the indicated speeds-to-fly and crab angles will remain invariant with altitude. This can be deduced from Figures 5 and 6 in which, for example, the indicated speed-to-fly and crab angle in 60 knot winds at 700-mb are comparable to those required in 91.6 knot winds at the 300- mb level.

Figures 5c and 6c show the maximum possible inverse glide slopes (L/D) if exact adherence to speed-to-fly and optimal crab angle is maintained. Clearly strong headwind conditions should be avoided since the L/D falls catastrophically from 47.7 in still air to less than 15 for the Nimbus IIb with 90 knot headwinds at 300- mb. It is also apparent that strong crosswinds exert a severe degradation of the glide slope in the absence of lift. Conversely, a 60 knot direct tailwind at 700- mb or a 91.6 knot tailwind at 300- mb will improve the L/D from 47.7 in still air to 92.7. Again, if a vertical wind gradient is present which obeys Long's solution, then the maximum possible inverse glide slope remains invariant with altitude. If on the other hand, an insulation layer is encountered in which the winds do not increase with altitude, flatter glide slopes are achieved for any given tailwind and direction at lower altitudes. If it is necessary to fly in a direct crosswind through an insulation layer, flatter glide slopes will be achieved at higher altitudes for any given wind speed. This is due to the fact that higher effective wing loadings at higher altitudes are an advantage for situations requiring penetration performance, as in a headwind or a strong crosswind, but a disadvantage when gliding slowly at

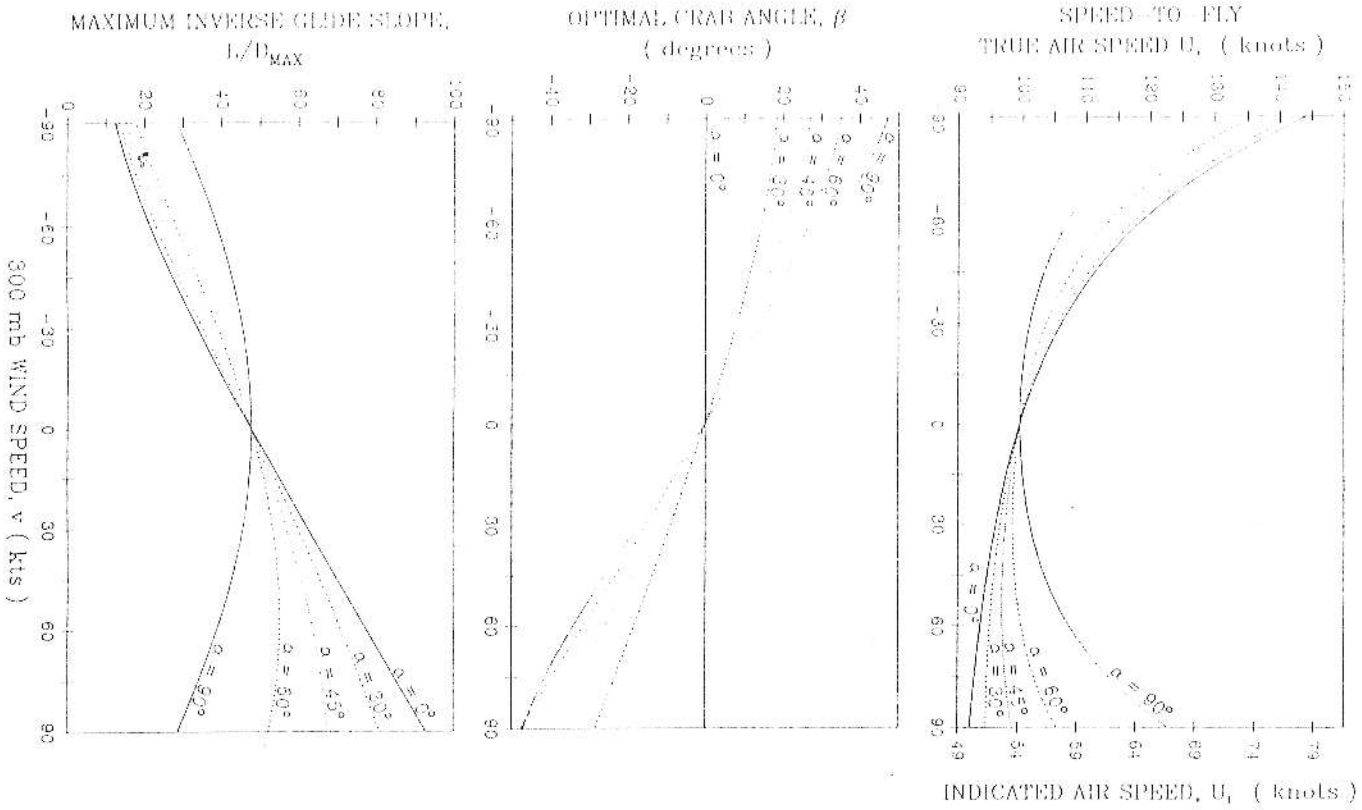

FIGURE 6: a) Speed-to-fly in the absence of lift as a function of wind speed and direction at the 300-mb level (33,000 ft MSL); b) Optimal crab angle in the absence of lift as a function of wind speed and direction at the 700-mb level (10,000 ft MSL); c) Maximum obtainable L/D in the absence of lift as a function of wind speed and direction at the 300-mb level (33,000 ft MSL).

minimum relative sinking speeds with the wind, see Jenkins and Wasyl (1990).

Figures 7a and b show computations of speed-to-fly and optimal crab angles for the case of quartering headwinds and tailwinds at the 500- mb level when vertical airmass movements are encountered. Contour plots are shown for particular airmass sink rates of $-1.0 \leq S \leq 8.0$ knots, as would be typically encountered while traversing mountains in fields of lee waves. Computations for an airmass rising faster than the aircraft's minimum relative sinking speed are not possible because a state of perpetual motion is achieved at the start of the seeded iteration, $v = v_o$ for which the problem has not been correctly posed by equation 8. The problem in this case becomes one of maximizing climb rate for which the speed-to-fly is $U \rightarrow u_s$. Otherwise, the speed-to-fly solutions in Figures 7a and b require one to speed up in sinking air and to slow down in rising air, similar to MacCready theory. However, unlike MacCready's original results, the speeds-to-fly for any given air mass sink rate are dependent upon the wind speed, requiring faster glides for a headwind component and slower glides with a tailwind component. Regardless of the air mass sink rate, speeds-to-fly in strong quartering tailwinds tend to increase slightly with increasing wind speed in order to prevent glideslope degradations resulting from excessively large crab angles, O(45°). This result is a modification to Kuettner's original downwind strategy. In strong quartering headwinds with a rapidly sinking air mass one finds in Figure 7a that rather large speeds-to-fly, O(200 knots), are required that exceed the structural load limits of most sailplanes. In 1 knot rising air with a quartering tailwind, the speed-to-fly is less than best L/D speed for still air.

Figures 8a and b show the effect of vertical air mass movements on speeds-to-fly and optimal crab angles in direct crosswinds at the 500- mb level. In strong direct crosswinds with rapidly sinking air, the speeds-to-fly are significantly less than the corresponding quartering headwind cases in Figure 7a but also significantly greater than the corresponding tailwind cases. For weak direct crosswinds ($v < 30$ knots) there is little change in speed-to-fly with increasing or decreasing wind speed, since most of the compensation is done with the crab angle. Unlike all other cases considered, the optimal crab angle for strong direct crosswinds ($v > 60$ knots) does indeed exceed 45 ° in non-sinking air.

Figures 7c and 8c show the maximum obtainable inverse glide slopes with vertical air mass motion in quartering headwinds and tailwinds and in direct crosswinds, respectively, at the 500 mb level. The computations are based on exact adherence to speed-to-fly and optimal crab angle according to Figures 7a, 7b, 8a and 8b. One finds that slowly rising air, S = -1 knot, yields impressive L/D for both strong quartering tail winds (L/D about 190) as well as weak crosswinds (L/D ~140). However, 100 kt quartering headwinds degrade the L/D to < 10 regardless of the vertical air mass motions, see Figure 7c. In fact, the inverse glide slope in this case is almost as bad for 8 knots of air mass sink as it would be for non-sinking air. The degradation in L/D for strong direct crosswinds is only slightly less, see Figure 8c. For weak quartering headwinds/tailwinds and direct crosswinds, any rate of sinking of the air mass exerts a pronounced

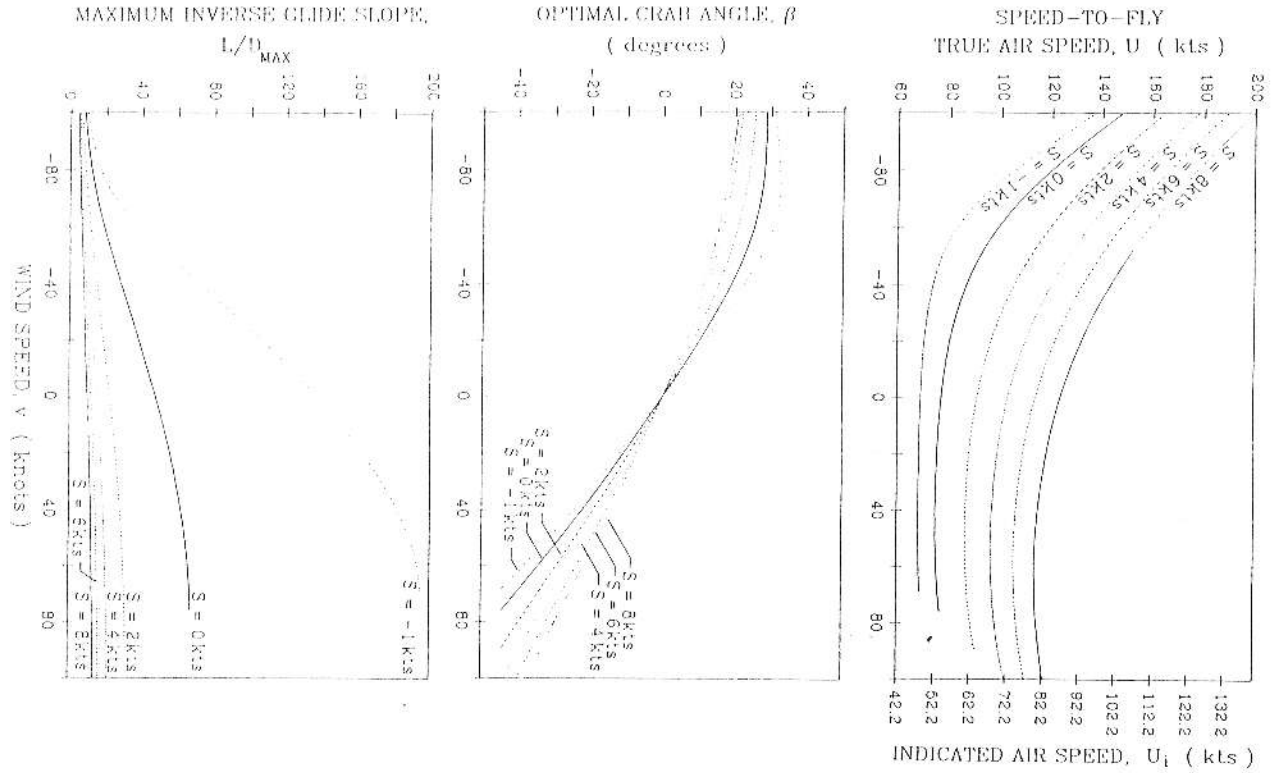

FIGURE 7: a) Speed-to-fly in quartering winds with vertical air mass motions at the 500-mb level (18,000 ft MSL); b) Optimal crab angles in quartering winds with vertical air mass motions at the 500-mb level (18,000 ft MSL); c) Maximum obtainable L/D in quartering winds with vertical air mass motion at the 500-mb level (18,000 ft MSL).

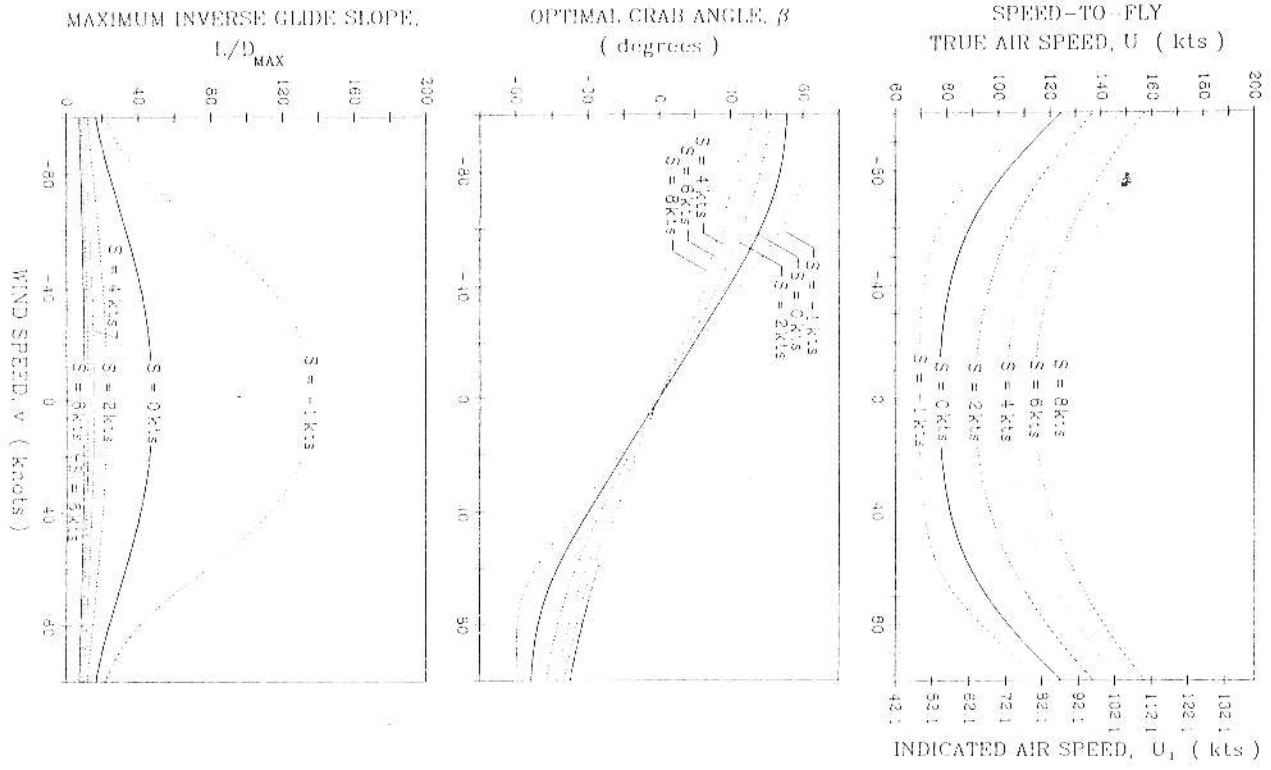

FIGURE 8: a) Speed-to-fly in direct crosswinds with vertical air mass motions at the 500-mb level (18,000 ft MSL); b) Optimal crab angles in direct crosswinds with vertical air mass motion at the 500-mb level (18,000 ft MSL); c) Maximum obtainable L/D in direct crosswinds with vertical air mass motions at the 500-mb level (18,000 ft MSL).

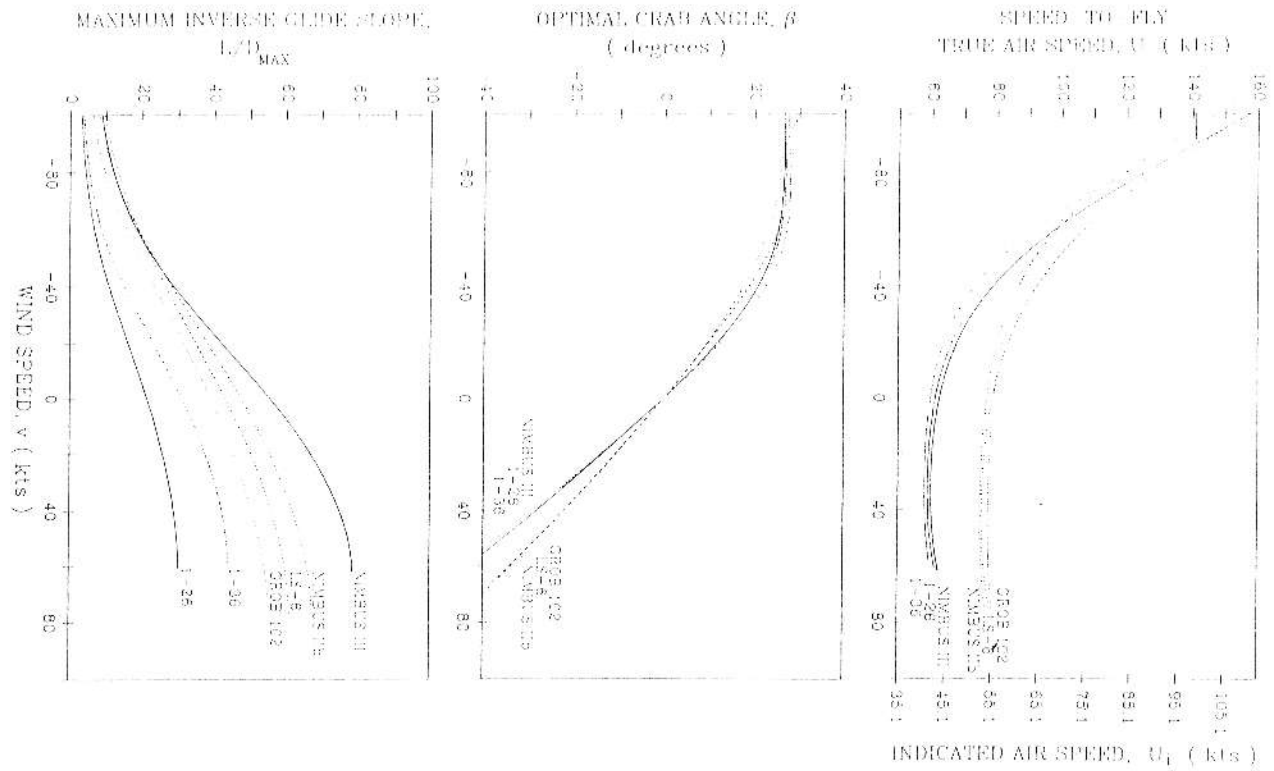

FIGURE 9: a) Speeds-to-fly for production sailplanes in quartering winds without lift, S + 0 at the 500-mb level (18,000 ft MSL). Calculations are based upon unballasted wing loadings with a 200 lb pilot and chute; b) Optimal crab angles for production sailplanes in quartering winds without lift, S = 0 at the 500-mb level (18,000 ft MSL). Calculations are based upon unballasted wing loadings with a 200 lb pilot and chute; c) Maximum obtainable L/D for production sailplanes in quartering winds without lift, S= 0, at the 500-mb level, (18,000 ft MSL). Calculations are based upon unballasted wing loadings with a 200 lb pilot and chute.

reduction in L/D compared to the case S = 0. Most of this performance loss occurs during the first few knots of air mass sink. Very little additional loss occurs for S ≥ 4 knots.

These solutions were verified in test flights by Jenkins and Wasyl (1990) in which known speed-to-fly errors were flown between the 700- and 300- mb levels. The loss in L/D due to any given speed-to-fly error was found to be greater at lower altitudes for both quartering tailwinds and direct crosswinds. Furthermore, flying too slowly produced a greater degradation in L/D than flying too fast. Speed-to-fly errors had a greater adverse impact in quartering tailwinds than in direct crosswinds. However, in either case, the speed-to-fly errors resulting from flying too slowly diminished the L/D by 15 points or more. Therefore, speed-to-fly errors which accumulate over long cross country wave flights represent significant glide slope degradations which may result in unnecessary and potentially dangerous losses in altitude or distance.

VII COMPARATIVE ANALYSIS

Here, we invoke the numerical variational solution from the Numerical Variational Solutions to explore the performance capabilities and speed-to-fly requirements of production aircraft across a rather broad spectrum of wing spans. At the upper limit of that spectrum we consider the example of the Schempp-Hirth Nimbus III, with a wing span of 24.5 m (80.3 ft.). The lower limit is bounded by the Schweizer 1-26, whose wing span is only 12.2 m (40.0 ft.). In the middle of our size spectrum lies the rather diverse band of 15 meter and standard class racers. We shall bracket this band with the Rolladen-Schneider LS-6 for the upper limit and the Grob 102 for the lower limit. To further resolve the size spectrum, we include calculations for the Schempp-Hirth Nimbus IIb (20.6 m or 66.6 ft. span), and the Schweizer 1-36 (14.1 m or 46.2 ft. span). A comparative summary of leading order physical characteristics for these aircraft is given in Table 1. Typically, we find that longer wing spans render higher aspect ratios.

We shall discuss our comparative calculations of these aircraft under two distinct sets of circumstances: 1) oblique downwind or upwind glides such as (B,G) in Figure 1; and 2) direct crosswind glides such as A', B') in Figure 1 performed in the absence of wave lift. Comparisons for glides performed directly with or against the wind such as (A,B') or (A',B) in Figure 1, are adequately presented in Reichmann (1975) and Kuettner (1985).

A) Oblique Downwind and Upwind Glides

Figure 9 gives calculations for the speed-to-fly requirements and maximum obtainable inverse glide slopes in the absence of lift (S=0), at the 500- mb level in quartering headwinds and tailwinds. The calculations are based upon the quadratic approximation to unballasted glide polars for each sailplane in our size spectrum, as derived in Appendix I. Generally, we find that flatter glide slopes, and thus, greater cross country distances, are achieved with higher aspect ratios, see Table 1. This performance advantage improves with either increasing tailwind component or diminishing crosswind component. However, the ultra-high aspect ratios (28-33) of open class sailplanes appear to give up a slight performance advantage to the more moderate aspect ratios (21-23) of 15 meter racing class sailplanes in the presence of strong headwind components. The threshold wind speed for this 15 meter dominance increases slightly with increasing

SAILPLANE MODEL	WING SPAN m (ft)	ASPECT RATIO	MAXIMUM AIRFOIL THICKNESS %	MINIMUM WING LOADING NT/m^2 (lb/ft^2)	ASPECT WING LOADING NT/m^2 (lb/ft^2)	MINIMUM SINK RATE (kts)	BEST L/D SPEED (kts)
Nimbus III	24.5 (80.3)	32.3	14.4	272 (5.69)	8.43 (0.176)	0.85	43
Nimbus II	20.6 (67.6)	28.6	17.0	310 (6.47)	10.82 (0.226)	0.95	50
LS-6	15.0 (49.2)	21.4	14.0	309 (6.46)	14.46 (0.302)	1.17	53
Grob 102	15.0 (49.2)	18.2	19.8	273 (5.71)	15.03 (0.314)	1.26	50
1-36	14.1 (46.2)	15.15	16.3	242 (5.05)	15.94 (0.333)	1.30	42
1-26	12.2 (40.0)	10.0	12.3	210 (4.38)	20.97 (0.438)	1.72	43

TABLE 1: Physical and performance characteristics of selected production sailplanes.

obliquity, ranging from 50 knots for a 30 degree headwind to about 60 knots for a 60 degree headwind. For oblique headwinds in excess of these thresholds, the maximum inverse glide slopes achieved with low aspect ratios (Less than 18), are remarkably poor, and potentially dangerous if landing sites are not within some distance of the same order as the available altitude.

It is interesting to examine the tendencies of speed-to-fly and optimal crab angles which occur across the size spectrum during oblique up wind and downwind glides in the absence of lift (S=0), see Figure 9. In strong quartering headwinds, there is only a 10 knot difference in speed-to-fly across the size spectrum, with the aircraft having the thinnest wings requiring the highest speeds and smallest crab angles, see Table 1. Remarkably, the speed-to-fly and optimal crab angles segregate into two distinct groups for weak quartering headwinds and for all quartering tailwinds. This segregation seems to occur in response to wing loading, with the low wing loading aircraft (less than 6 lbs/ft²) forming a low speed, high crab angle group. Segregation appears to be totally independent of aspect ratio or maximum obtainable inverse glide slope, see Table 1.

B) Direct Crosswind Glides

Some of the trends observed in oblique glides are found to persist in direct crosswind glides. The wind speeds for particular behavior are slightly different. In Figure 10a, we calculate size variation in the maximum obtainable inverse glide slopes for direct crosswinds at the 500 mb level in the absence of lift (S=0). For weak to moderate crosswinds (less than 60 knots) there exists a progressive improvement in glide efficiency with increasing aspect ratio. As the crosswind velocity exceeds 60 knots, there is a gradual reversal of this trend as the ultra-high aspect ratio performance is successively exceeded by the performance of more moderate aspect ratios. Above crosswind speeds of 70 knots, the 15 meter racing class exhibits a slight advantage over the open class.

The along course speeds realized by exact adherence to speed-to-fly and optimal crab angle are calculated in Figure 10b for direct crosswinds at the 600 mb level. These are the ground speeds that are achieved at the maximum inverse glide slopes calculated in Figure 10a. For weak to moderate crosswind speeds (less than 50 knots) we find that the along course speeds segregate roughly into two groups according to wing loading. Aircraft whose loadings are less than 6 lbs/ft² tend to group together at relatively slower along course speeds than those greater than 6 lbs/ft², regardless of aspect ratio or maximum inverse glide slope. In strong direct crosswinds (greater than 80 knots), the along course speeds are ordered according to the relative wing thickness, see Table 1. Again this ordering is irrespective of maximum inverse glide slope. The minimum along course speed at the transition to strong direct crosswind speeds (50 to 70 knots) occurs where the crab angle solution begins to flatten, see figure 8b. consequently, further corrections to maintain course heading with increasing wind speed are accomplished by flying faster,

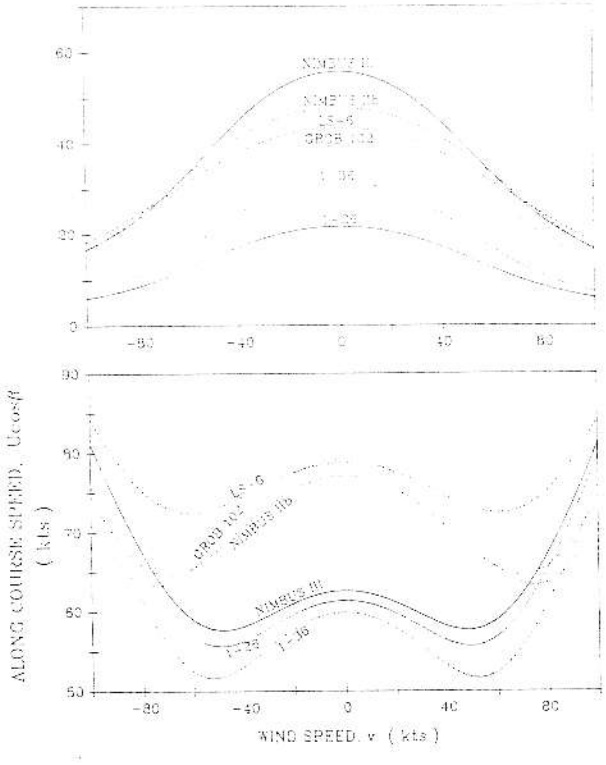

FIGURE 10: a) Maximum obtainable L/D for production sailplanes in direct crosswinds without lift, S = 0, at the 500-mb level (18,000 ft MSL). Calculations are based upon unballasted wing loadings with a 200 lb pilot and chute; b) Maximum obtainable along-course speeds for production sailplanes in direct crosswinds without lift, S = 0, at the 500-mb level (18,000 ft MSL). Calculations are based upon unballasted wing loadings with a 200 lb pilot and chute.

giving a subsequent increase in along course speed. In the regime of weak to moderate crosswinds (less than 50 knots) the speeds-to-fly remain relatively constant, such that subsequent increases in windspeed are compensated with increases in crab angle and corresponding reductions in along course speed.

C) Discussion

The results of the comparative analysis can be understood in terms of the general polar equations, (21)-(23) in Appendix I. For any given wind field, individual aircraft performance is determined by an induced drag term (proportional to K4) which dominates at low speeds and a profile drag term (proportional to K3) which dominates at high speeds. Speed-to-fly solutions with tailwinds and weak crosswind components are found to exploit the low speed portion of the glide polar where induced drag effects are the primary constraint on performance. Arguing from classical lifting line theory, the factor K4 is inversely proportional to the aspect ratio at the lowest order approximation, Van Dyke (1964). the induced drag is also linearly proportional to the wing loading, see equation (23). Therefore, the glide efficiency at low speed is governed primarily by the ratio of the wing loading to the aspect ratio, termed "aspect wing loading" in Table 1. We find that the maximum inverse glide slope with tailwind or weak crosswind components progressively increases with decreasing aspect wing loadings. Consequently, the critical design considerations for maximizing cross country distance in either oblique or direct downwind wave flights should be focused on maximizing aspect ratio while maintaining the lowest possible wing loading.

The segregation of speed-to-fly and along course speed according to wing loading for tailwind or weak crosswind components is also a low speed phenomena dominated by induced drag effects. The quest for higher aspect ratios to minimize induced drag also tends to increase wing loading, especially in the absence of advanced composites (Nimbus IIb and Grob 102) or under the constrain of a fixed wing span (LS-6). The polar coefficients (a,b,c) are altered by the wing loading according to equation 24 such that higher wing loadings give higher glide speeds over the entire polar. Higher glide speeds in the low speed portion of the polar in turn diminish the induced drag term in equation 21 and thereby improve glide efficiencies. Therefore, the high wing loading aircraft must fly faster to achieve maximum efficiency in the low speed portion of the polar. This is reflected in the results in Table 1 where the high best L/D speeds are found to correlate with high wing loadings.

In strong headwinds and crosswinds, the speed-to-fly solutions require utilization of the high speed portion of the polar. Here the profile drag term in equation (21) controls performance characteristics. Since the induced drag term becomes small, the aspect ratio exerts a minimal favorable effect. Instead, the wing thickness becomes the controlling length scale in the profile drag factor, K1, see Van Dyke (1964). The degree of sophistication of the airfoil technology in maximizing the extent of laminar boundary layers also has an important effect on the size of the profile drag exponent. If the boundary layers can be maintained, laminar over the entire airfoil, then the profile drag exponent approaches the theoretical maximum of 1/2 and the profile drag contributions to the sinking speed increases only as the 2.5 power of the glide speed. If, on the other hand, the boundary layers are everywhere turbulent over the airfoil, then the profile drag exponent approaches 1/5 and the profile drag influence on the sinking speed grows more rapidly, as the 2.8 power of the glide speed. In addition to these airfoil factors of thickness and shape, the profile drag term in equation 22 also decreases with increasing wing loading. Therefore, the loss of the performance advantage of open class sailplanes in strong headwind and crosswind components is due to a combination of factors: 1) they are deriving a minimal advantage from their high aspect ratios, while; 2) they are suffering from thick airfoils necessary for adequate bending strength at high aspect ratios (Nimbus IIb); or 3) their wing loading is too low (Nimbus III). Clearly, the third factor could be corrected by ballasting. Consequently, for crosswind wave flights or for speed triangles where legs must be flown into the wind, the leading order design criteria is a thin, modern airfoil (LS-6) which employs advanced pressure recovery buckets or boundary layer control to minimize profile drag.

To determine ballast effects in severely oblique winds we calculate in Figure 11 the maximum obtainable inverse glide slopes at minimum wing loadings with a 200 lb. pilot and parachute versus those at maximum certified gross weight. The calculations are performed for open and 15 meter racing class examples gliding in the absence of lift at the 500 mb level with winds blowing at 60 degrees across the course line. Naturally ballasted configurations achieve higher inverse glide slopes than those which are unballasted when flying into a headwind component. The 15 meter dominance into strong headwinds is still present, but at a much higher threshold windspeed (80 knots) and to a greatly diminished degree. Since both the Nimbus III and LS-6 have comparably

thin wings, this strong head wind advantage of the 15 meter example is probably due to the slightly higher maximum wing loading. The most surprising result is the performance advantage realized by ballasting in strong oblique tailwinds in excess of 50 knots. This occurs when required speeds-to-fly begin to increase to avoid excessive crab angles, see Figures 5 and 6. At these higher speeds-to-fly, the profile drag term in Equation 21 becomes large and ballasting then provides a reduction in sinking speed and, hence, improved glide slope.

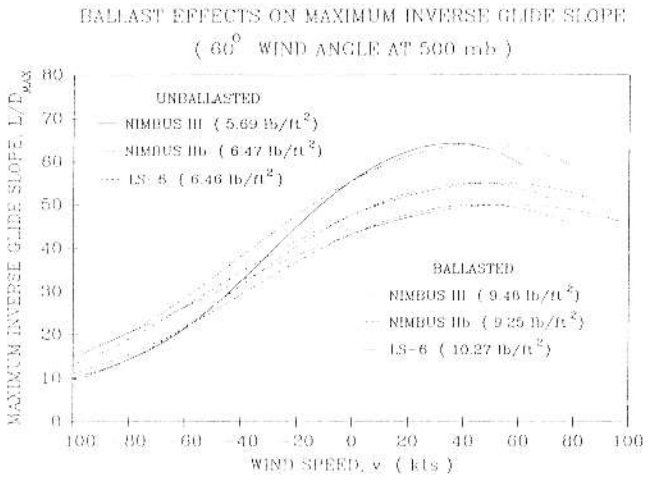

FIGURE 11: Maximum obtainable L/D for production sailplanes with and without ballast in severely oblique winds without lift S = 0, at the 500-mb level (18,000 ft MSL). Unballasted calculations are based upon factory claims of empty weight plus a 200 lb pilot and chute. Ballasted calculations are based upon maximum certified gross weights.

CONCLUSIONS

From the preceding results, we conclude that cross country wave flights may be optimized by the following selection of tactics and equipment:

1) Speed-to-fly during glides skewed relative to the wind by less than 60° requires flying faster through sinking air or into headwind component and flying slower through rising air or with a tailwind component such that the crab angle does not become excessively large, less than 0(45°).

2) Speed-to-fly in severely oblique winds (wind angles greater than 60°) requires flying faster through sinking air or with increasing wind speed and flying slower through rising air or with decreasing wind speed, using crab angles that may exceed 45° for the case of strong wind in a non-sinking air mass.

3) Indicated speeds-to-fly decrease with altitude in the absence of wind gradients aloft (insulation layers).

4) Indicated speeds-to-fly remain invariant with altitude when wind gradients aloft satisfy Long's solution.

5) Maximum L/D with any given tailwind component in an insulation layer is achieved at lower altitudes.

6) Maximum L/D with any given headwind component or any given direct crosswind in an insulation layer is achieved at higher altitudes.

7) Speed-to-fly errors resulting from flying too slowly yield the greatest losses in L/D.

8) Losses in L/D for any given speed-to-fly error are greater at lower altitudes.

9) High aspect ratios and low wing loading progressively increase the maximum obtainable L/D with increasing tailwind and diminishing crosswind components.

10) Thin airfoils and high wing loadings yield the flattest glide slopes with increasing headwind and crosswind components.

11) Ballasting is advantageous in oblique headwinds, direct crosswinds and strong oblique tailwinds.

REFERENCES

Basu, B.C. and G.J. Hancock, 1978, "The Unsteady Motion of a Two-dimensional Aerofoil in Incompressible Inviscid Flow," Journal of Fluid Mechanics, vol. 87, no. 1, pp. 159-178.

Gill, A.E., 1982, Atmosphere - Ocean Dynamics, Academic, Orlando, FL, pp. 274-294.

Huth, H., 1963, "Proleme des Leistungssegelfluges," Deutscher Aeroclub, vol. 3, pp. 72-77.

Irving, F.G., 1974, "Altitude Effect on Variometers," 14th OSTIV Congress, Waikerie, Australia and Technical Soaring, vol. III, no. 2, pp. 31-35.

Jenkins, S.A. and J. Wasyl, 1990, "Optimization of Glides for Constant Wind Fields and Course Headings," Journal of Aircraft, vol. 27, no. 7, pp. 632-638.

Johnson, R.E., 1977, "Flight Test Polar Measurements of Modern Sailplanes," Technical Soaring, vol. 4, no. 4, pp. 13-27.

Johnson, R.H., 1977, "A Flight Test Evaluation of the Schweizer 1-26E," The Johnson Flight Tests, Soaring Society of America, pp. 74-77.

Johnson, R.H., 1982a, "A Flight Test Evaluation of the Schweizer 1-36, Soaring, vol. 46, no. 3, pp. 35-38.

Johnson, R.H., 1982b, "A Flight Test Evaluation of the Nimbus III," Soaring, vol. 46, no. 12, pp. 18-24.

Johnson, R.H., 1984, "A Flight Test Evaluation of the Grob 102," Soaring, vol. 48, no. 1, pp. 18-23.

Kuettner, J.P., 1985, "The 2000 Kilometer Wave Flight - Part II," Soaring, vol. 49, no. 3, pp. 22-27.

MacCready, 1954, P.B., "Optimum Airspeed Selector," Soaring, vol. 18, no. 2, pp. 16-21.

MacCready, P.B., 1982, "Understanding Speed-to-fly and the Speed Ring," Soaring, vol. 47, no. 5, pp. 42-47.

Prandtl, L., 1931, Abriss der Stromungslegre, Vieweg, Braunschweig, FRG, p. 189.

Reichmann, H., 1975, "Zum Problem der Fahrtoptimierun im Streckensegelflug," Ph.D. dissertation, Universitat Karlsuruhe, pp. 233.

Reichmann, H., 1978, Cross-Country Soaring, Thomson, Pacific Palisades, CA, p. 98.

Rolladen-Schneider, 1987, "The World Champion LS-6," Rolladen Schneider Flugzeugbau GmbH, Egelsbach, Germany.

Van Dyke, M., 1964, "Lifting Line Theory as a Singular-Perturbation Problem," Journal of Applied Mathematics and Mechanics, Vol. 28, pp. 90-101.

APPENDIX 1: Derivation of the Quadratic Glide Polar

The vertical and horizontal components of the glide velocity relative to the air mass are related by the glide polar at sea level in still air. This relation can be posed from the usual assumption that the total drag is a linear combination of profile drag and induced drag:

$$C_D = C_{D,P} + C_{D,i} \qquad (18)$$

Because of Reynolds number dependence, the profile drag coefficient is not constant but will vary with the glide velocity in still air at sea level $\hat{u}$ according to

$$C_{D,P} = K_1 \hat{u}^{-\gamma} \qquad (19)$$

where K_1 is a factor that varies with the kinematic viscosity and characteristic length scale and γ will depend on the relative proportion of the total wetted surface area that is subjected to laminar vs turbulent boundary layers. The induced drag coefficient on the other hand may be inferred from lifting line theory (Prandtl, (1931) and Van Dyke (1964)) as

$$C_{D,I} = K_2 C_L^2 \tag{20}$$

where the factor K_2 is a function of wing aspect ratio, twist, taper and aeroelasticity. Based upon a drag formulation by equations 18-20, the glide polar at sea level may be written as

$$w = (C_D/C_L)\ U = K_1 U^{1-\gamma} + (K_4/U) \tag{21}$$
$$K_1 = (\hat{\rho} A_0 K_1)/(2m) \tag{22}$$
$$K_4 = (2mK_2)/(\hat{\rho} A_0) \tag{23}$$

If we expand equations 21-23 in a Taylor series about some optimal speed-to-fly in still air, $\hat{u} = \hat{U}$ then the glide polar is quadratic to second order according to

$$K_1 U^{1-\gamma} + (K_4/U) = \hat{a}U^2 + \hat{b}U + \hat{c} \tag{24}$$

where

$$\hat{a} = (3-\gamma)(2-\gamma) K_1 \hat{U}^{1-\gamma} + (2K_4/\hat{U}^3)$$

$$\hat{b} = (3-\gamma) K_1 \hat{U}^{2-\gamma} - (K_4/\hat{U}^2) - 2\hat{U}\hat{a}$$
$$\hat{c} = K_1 \hat{U}^{3-\gamma} + (K_4/\hat{U}) + \hat{a}\hat{U}^2 - \hat{b}\hat{U}$$

Here $\hat{a}$,$\hat{b}$, and $\hat{c}$ are based on the air density at sea level. We may then correct the quadratic glide polar in equation 24 to any altitude where the air density is p by taking

$$w = au^2 + bu + c \tag{25}$$
$$a = \hat{a}(\hat{\rho}/\rho)^{-1/2} \tag{26}$$
$$b = \hat{b} \tag{27}$$
$$c = \hat{c}(\hat{\rho}/\rho)^{1/2} \tag{28}$$

A comparison is shown in Jenkins and Wasyl (1990) between the quadratic approximation according to equation 24 and measured glide polar data for a Schempp-Hirth Nimbus IIb, taken from Johnson (1977) and corrected to sea level. The values for the sea level polar coefficients that result from this fit are

NIMBUS IIb:

$$\hat{a} = 0.0012155\ kt^{-1} \tag{29}$$
$$\hat{b} = -0.1106912 \tag{30}$$
$$\hat{c} = 3.564157\ kt \tag{31}$$

Corrected glide polars for the 700-, 500- and 300- mb altitudes are also shown in Jenkins and Wasyl (1990). The maximum inverse glide slope of 47.7 were found to remain unchanged with altitude for still air. The deformation of the polar at altitude is equivalent to increasing the wing loading by factors of 1.20, 1.42 and 1.84 for the 700-, 500- and 300- mb levels, respectively.

The quadratic approximation applied to published flight test data from Rolladen-Schneider (1987) and Johnson (1977, 1982a, 1982b and 1984) yields the additional sets of sea level polar coefficients for the remaining aircraft discussed in section VII.

NIMBUS III:

$\hat{a} = 0.00089\ kt^{-1}$, $\hat{b} = -0.05504$, $\hat{c} = 1.604653\ kt$

LS-6:

$\hat{a} = 0.000853\ kt^{-1}$, $\hat{b} = -0.071319$, $\hat{c} = 2.61027\ kt$

GROB 102:

$\hat{a} = 0.001745\ kt^{-1}$, $\hat{b} = -0.108731$, $\hat{c} = 5.400708\ kt$

1-36:

$\hat{a} = 0.00211\ kt^{-1}$, $\hat{b} = -0.145559$, $\hat{c} = 3.73199\ kt$

1-26:

$\hat{a} = 0.002372\ kt^{-1}$, $\hat{b} = -0.159231$, $\hat{c} = 4.409795\ kt$

Clearly, the aircraft with the highest glide efficiencies are those having the smallest absolute values of polar coefficients.